

# Evidence for an environment-dependent shift in the baryon acoustic oscillation peak

Boudewijn F. Roukema<sup>1,2\*</sup>, Thomas Buchert<sup>2</sup>, Jan J. Ostrowski<sup>1,2</sup>,

Martin J. France<sup>2</sup>

<sup>1</sup> *Toruń Centre for Astronomy, Faculty of Physics, Astronomy and Informatics, Nicolaus Copernicus University, ul. Gagarina 11, 87-100 Toruń, Poland*

<sup>2</sup> *Université de Lyon, Observatoire de Lyon, Centre de Recherche Astrophysique de Lyon, CNRS UMR 5574: Université Lyon 1 and École Normale Supérieure de Lyon, 9 avenue Charles André, F-69230 Saint-Genis-Laval, France†*

Le 1 mai 2015

## ABSTRACT

The Friedmann–Lemaître–Robertson–Walker (FLRW) metric assumes comoving spatial rigidity of metrical properties. The curvature term in comoving coordinates is environment-independent and cannot evolve. In the standard model, structure formation is interpreted accordingly: structures average out on the chosen metrical background, which remains rigid in comoving coordinates despite nonlinear structure growth. The latter claim needs to be tested, since it is a hypothesis that is not derived using general relativity. We introduce a test of the comoving rigidity assumption by measuring the two-point auto-correlation function on comoving scales—assuming FLRW comoving spatial rigidity—in order to detect shifts in the baryon acoustic oscillation (BAO) peak location for Luminous Red Galaxy (LRG) pairs of the Sloan Digital Sky Survey Data Release 7. In tangential directions, subsets of pairs overlapping with superclusters or voids show the BAO peak. The tangential BAO peak location for overlap with Nadathur & Hotchkiss superclusters is  $4.3 \pm 1.6h^{-1}$  Mpc less than that for LRG pairs unselected for supercluster overlap, and  $6.6 \pm 2.8h^{-1}$  Mpc less than that of the complementary pairs. Liivamägi et al. superclusters give corresponding differences of  $3.7 \pm 2.9h^{-1}$  Mpc and  $6.3 \pm 2.6h^{-1}$  Mpc, respectively. We have found moderately significant evidence (Kolmogorov–Smirnov tests suggest very significant evidence) that the BAO peak location for supercluster-overlapping pairs is compressed by about 6% compared to that of the complementary sample, providing a potential challenge to FLRW models and a benchmark for predictions from models based on an averaging approach that leaves the spatial metric *a priori* unspecified.

**Key words:** cosmology: observations – large-scale structure of Universe – distance scale – cosmological parameters – dark energy

## 1 INTRODUCTION

The low-redshift ( $z \ll 3$ ) Universe has an inhomogeneous density distribution (e.g. de Lapparent et al. 1986), i.e. during the epoch when most virialisation takes place. The standard cosmology model assumes that the nonlinear structure growth of the virialisation epoch takes place in a spacetime with the Friedmann–Lemaître–Robertson–Walker (FLRW) metric, and that this metric is unaffected by structure growth, despite the Einstein equation. In other words, an implicit assumption of the FLRW models, including the  $\Lambda$ CDM model (e.g. Ostriker & Steinhardt 1995; Spergel et al. 2003; Ade et al. 2014), is that comoving space is rigid, a property

that is shared by Newtonian models (see Sect. 2.5 in Buchert 2000, and (Roukema 2013)). This assumption needs to be tested. We propose to test the rigidity of a well-established comoving-scale standard ruler, by examining whether it is environment-dependent.

Motivated by Ellis & Stoeger (1987), the scalar averaging approach to cosmology (Buchert, Kerscher & Sicka 2000; Buchert 2000, 2001; Kolb et al. 2005; Kolb, Matarrese & Riotto 2006; Räsänen 2006a,b; Buchert, Larena & Alimi 2006; Wiltshire 2007a,b; Buchert 2008; Buchert & Carfora 2008; Wiltshire 2009; Kolb 2011; Buchert, Nayet & Wiegand 2013; Duley, Nazer & Wiltshire 2013) is a general-relativistic approach to cosmology that extends the Friedmann and acceleration equations to the case of general inhomogeneous distributions of matter *and geometry*. Initial observational tests show promising results for template metric implementations of the approach and for related toy models (e.g. Larena et al. 2009;

\* In memory of my father, Arie Roukema, who made me curious about the fundamental properties of the Universe.

† BFR: during visiting lectureship; JJO: during long-term visit.

Roukema, Ostrowski & Buchert 2013; Boehm & Rasanen 2013; Chiesa et al. 2014; see also models with the inclusion of a phenomenological lapse function: Smale & Wiltshire 2011; Wiltshire et al. 2013 or using a different averaging approach: Clarkson et al. 2012).

Comoving space in these approaches is not rigid. This implies that comoving standard rulers should be inferred to be variable in comoving length if data are interpreted according to a phenomenological, rigid model, e.g. a  $\Lambda$ CDM model. It is generally expected (Hosoya et al. 2004; Räsänen 2006a; Buchert & Carfora 2008; Roukema et al. 2013) that voids should be hyperbolic and that superclusters should occupy positively curved space. This is a kinematical expectation, whose details depend on whether we interpret the backreaction variables in a background-free way, or whether we use template metrics to interpret those variables (Buchert & Carfora 2003). When using a template metric, or a best-fit FLRW metric, voids and superclusters and their nearby surroundings should approximately correspond to negatively curved, fast expanding regions and to positively curved regions approaching their turnaround epochs, respectively.

A comoving standard ruler at  $L \sim 100h^{-1}$  Mpc, the baryon acoustic oscillation (BAO) peak, has been detected to high statistical significance (Eisenstein et al. 2005, and references thereof), where the comoving length is determined from the theory of baryon acoustic oscillations (e.g. Eisenstein & Hu 1998, and references therein). Measuring the BAO peak location—an imprinted feature in comoving space—through either large voids or superclusters for a given catalogue interpreted in rigid (FLRW) comoving space should show either a stretched or compressed BAO peak location, respectively, in comparison to the BAO peak location for the full catalogue, interpreted in the same way. However, since voids dominate spatial 3-volume at the present epoch, the scalar averaging expectation is that the BAO peak location through large voids should only be *slightly* greater than that for the best-fit FLRW model (Buchert & Carfora 2008; Roukema et al. 2013), i.e. difficult to detect. Moreover, voids consist of deficits of galaxy densities rather than excesses of galaxy densities, so procedures of finding and characterising voids are more affected by Poisson noise than in the case of superclusters. Thus, the relative stretching of the BAO peak location through voids should be small compared to the best-fit FLRW model, and noisy.

As a rough guide to what could be expected in the scalar averaging case, we prepared an independent software package that implements the calculations illustrated in Fig. 2 (left) of Buchert et al. (2013) for the relativistic Zel’dovich approximation (Kasai 1995; Buchert & Ostermann 2012) together with an early-epoch background model (Buchert et al. 2013). We find that present-day effective (averaged) expansion factors  $a_{\text{eff}}$  of typical ( $1\sigma$  in the first invariant of the extrinsic curvature tensor and zero in the second and third invariants; see Buchert et al. 2000, 2013 for details) overdense or underdense regions at the  $105h^{-1}$  Mpc scale have effective scale factors of 0.95 or 1.04 times that of the extrapolated background model, i.e. the overdense region is about 9% compressed in comparison to the underdense region. The relative compression is the relevant quantity to consider here.

Instead of checking whether the BAO peak location through voids is stretched, a more promising approach is to use superclusters. Lines of sight passing through superclusters should pass through the compressed spatial regions, while lines of sight mostly passing far from the superclusters should pass mostly through negatively curved space, according to the scalar averaging models. While superclusters are unvirialised objects (typically of filamen-

tary or spiderlike morphology; e.g. Einasto et al. 2014), they should not dominate the volume, so the metrical properties of the space they occupy are more likely to differ from volume-weighted mean quantities than in the case of voids. Thus, we expect to find a stronger and less noisy shift in the BAO peak location from superclusters than from voids, and focus mostly on the former.

The BAO peak is well-determined in the Sloan Digital Sky Survey Release 7 (SDSS DR7) luminous red galaxy (LRG) sample (Eisenstein et al. 2001), with publicly available catalogues of both the observational data and of “random” galaxies representing the observational selection criteria. We use these to illustrate our method. We consider independent supercluster catalogues from Nadathur & Hotchkiss (2014) and Liivamägi, Tempel & Saar (2012), and Nadathur & Hotchkiss (2014)’s Type 1 void catalogue. The aim here is an initial exploration of the method using real observational catalogues, with the hope of detecting the BAO peak. The amplitude and sign of a shift in the BAO peak location or an upper limit to the shift should guide future work on observational catalogues that are presently being prepared for public release or that will result from the next generation of extragalactic telescope/instrument/survey combinations.

The observational catalogues are described in Sect. 2.1. The correlation function estimator is given in Sect. 2.2. The calculation of an overlap between an LRG pair and a supercluster (or void) in flat FLRW comoving space is given in Sect. 2.3 [Fig. 1, Eqs (5), (6), and (7)]. Determination of the BAO peak location and its shift is described in Sect. 2.4. Our method is conceptually simple but computationally heavy: numerical optimisation strategies are listed in Sect. 2.5.

Results are presented in Sect. 3 and discussed in Sect. 4. Conclusions are given in Sect. 5. Distances and separations are stated in FLRW comoving units except if stated otherwise, and  $\Omega_{m0}$  and  $\Omega_{\Lambda0}$  are the zero-redshift FLRW dimensionless matter density and dark energy density parameters, respectively. In terms of common terminology, the assumed comoving space is the FLRW space used by, for example, Nadathur & Hotchkiss (2014), i.e. neither “real space” (since peculiar velocities remain uncorrected for in the redshifts), nor “redshift space” (in the sense that  $cz$  is not used as the radial distance). The Hubble constant is written  $H_0 = 100h$  km/s/Mpc.

## 2 METHOD

### 2.1 Observational catalogues

We use the “bright” and “dim” LRG samples *lrgbright* and *lrgdim* derived from the SDSS DR7 (Eisenstein et al. 2001), as provided by Kazin et al. (2010) as observational and “random” catalogues for the “Northern Cap only”<sup>1</sup>. These are converted to Euclidean comoving positions

$$\begin{aligned} x_i^D &:= r_i^D \cos \alpha_i^D \cos \delta_i^D \\ y_i^D &:= r_i^D \sin \alpha_i^D \cos \delta_i^D \\ z_i^D &:= r_i^D \sin \delta_i^D, \end{aligned} \quad (1)$$

where  $r_i^D$  is the radial comoving distance in  $h^{-1}$  Mpc to the  $i$ -th LRG according to an FLRW model with ( $\Omega_{m0} = 0.32$ ,  $\Omega_{\Lambda0} = 0.68$ ).

Nadathur & Hotchkiss (2014)’s *v11.11.13* lists of superclusters identified using the watershed algorithm in LRG samples *lrgbright* and *lrgdim* derived from the SDSS DR7 (Eisenstein et al.

<sup>1</sup> <http://cosmo.nyu.edu/~eak306/SDSS-LRG.html>

**Table 1.** Numbers of SDSS DR7 Northern Galactic Cap LRGs and superclusters (Sect. 2.1)

subset <sup>a</sup>	$D^b$	$R^c$	ref
LRGs:			
dim	61899	3082871	Kazin et al. (2010)
bright	30272	1521736	Kazin et al. (2010)
superclusters:			
dim + bright	235		Nadathur & Hotchkiss (2014)
$z < 0.6^d$	2701		Liivamägi et al. (2012)
voids:			
dim + bright	83		Nadathur & Hotchkiss (2014)

<sup>a</sup>The “dim” and “bright” subsets of LRGs are defined by the authors of these analyses.

<sup>b</sup>“Data”: observed galaxies, as listed by Kazin et al. (2010).

<sup>c</sup>“Random”: galaxies simulated by Kazin et al. (2010) to mimic selection criteria. Randomly selected subsets of these are used in the present work.

<sup>d</sup>See Sect. 3.2 of Liivamägi et al. (2012) for details.

2001) are used here<sup>2</sup>. These include the right ascension and declination  $\alpha_j^{\text{SC}}, \delta_j^{\text{SC}}$ , effective radius  $R_j$  in  $h^{-1}$  Mpc and angular radii  $\theta_j^{\text{SC}}$  of the superclusters<sup>3</sup>, which are converted to Euclidean comoving positions as in Eq. (1), i.e.

$$\begin{aligned} x_j^{\text{SC}} &:= r_j^{\text{SC}} \cos \alpha_j^{\text{SC}} \cos \delta_j^{\text{SC}} \\ y_j^{\text{SC}} &:= r_j^{\text{SC}} \sin \alpha_j^{\text{SC}} \cos \delta_j^{\text{SC}} \\ z_j^{\text{SC}} &:= r_j^{\text{SC}} \sin \delta_j^{\text{SC}}, \end{aligned} \quad (2)$$

where radial comoving distances  $r_j^{\text{catalogue}}$  of the supercluster centres are derived as

$$r_j^{\text{catalogue}} = R_j / \tan \theta_j^{\text{SC}}, \quad (3)$$

the  $r_j^{\text{catalogue}}$  values are converted to redshifts for the authors’ FLRW model (with  $\Omega_{\text{m}0} = 0.27, \Omega_{\Lambda 0} = 0.73, h = 1.0$ ), and the latter are reconverted to radial comoving distances  $r_j^{\text{SC}}$  for the FLRW model chosen in this work ( $\Omega_{\text{m}0} = 0.32, \Omega_{\Lambda 0} = 0.68$ ). Nadathur & Hotchkiss (2014)’s void catalogues for SDSS DR7 LRGs are extracted in the same way.<sup>4</sup>

Nadathur & Hotchkiss (2014, Fig. 4) used a conservative sky selection mask, with a complicated sky geometry. Superclusters outside of the main (“Northern Galactic Cap”) SDSS sky region are excluded in this work (i.e. superclusters with centres not satisfying  $110^\circ < \alpha_j^{\text{SC}} < 260^\circ$  are ignored).

Liivamägi et al. (2012, Fig. 1) derived supercluster catalogues from the SDSS DR7, using a less stringent sky mask than Nadathur & Hotchkiss (2014). The celestial positions and FLRW radial distances of supercluster catalogue selected with an adaptive detection threshold<sup>5</sup> are analysed here, since this catalogue is found by the authors to approximate a volume-limited, distance-independent catalogue. As for the Nadathur & Hotchkiss (2014)

<sup>2</sup> <http://research.hip.fi/user/nadathur/download/dr7catalogue/>

<sup>3</sup> Columns 2, 3, 5, and 6, respectively, of the files `comovcoords/lrgdim/Type1clusters.info.txt` and `comovcoords/lrgbright/Type1clusters.info.txt`.

<sup>4</sup> Files `comovcoords/lrgdim/Type1voids.info.txt` and `comovcoords/lrgbright/Type1voids.info.txt`.

<sup>5</sup> Columns “RA1deg”, “DE1deg”, and “Dist1” of <http://cdsarc.u-strasbg.fr/viz-bin/nph-Cat/txt?J/A+A/539/A80/lrgadap.dat>, representing estimates for the primary peaks of the superclusters.

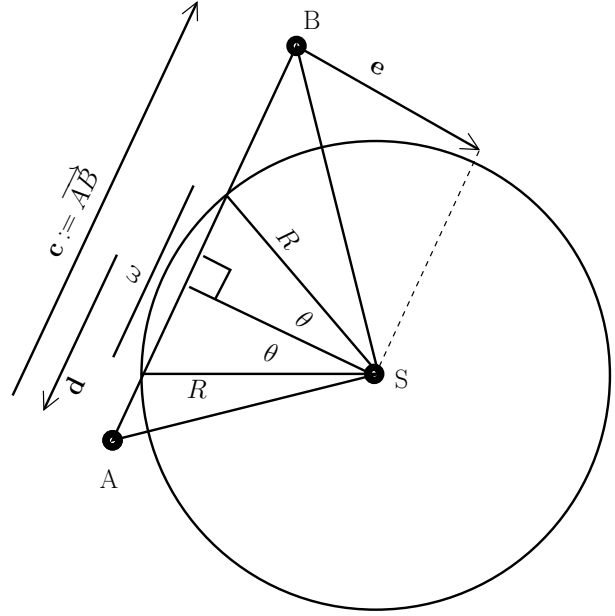


**Figure 1.** Geometrical definition of the overlap between a supercluster (or void) and an LRG–LRG pair in the comoving observational spatial section interpreted with an FLRW flat metric. Two LRGs are located at positions A and B, respectively; the supercluster (or void) is centred at S and assumed to be spherical, of radius  $R$ . The vector  $\mathbf{e}$  is normal to the pair separation vector  $\mathbf{c} := \overline{AB}$  and extends from the line segment  $\overline{AB}$  to the supercluster (void) centre S. In the case illustrated, the pair–supercluster overlap  $\omega$  is the chord length [Eq. 5]. See Sect. 2.3 for other cases.

catalogues, the catalogue FLRW radial distances are converted to redshifts using ( $\Omega_{\text{m}0} = 0.27, \Omega_{\Lambda 0} = 0.73, h = 1.0$ ) (Liivamägi et al. 2012; Sect. 3.1) in order to be consistent with those authors’ analysis of the observations. These inferred redshifts are then converted to radial comoving distances  $r_j^{\text{SC}}$  for the FLRW model chosen for this work ( $\Omega_{\text{m}0} = 0.32, \Omega_{\Lambda 0} = 0.68$ ). The Euclidean comoving positions follow from Eq. (2).

Table 1 lists the numbers of real galaxies, simulated galaxies, real superclusters, and real voids used in this work.

## 2.2 Correlation function $\xi(s)$

The two-point auto-correlation function  $\xi(s)$ , where  $s$  is the pair separation in FLRW comoving space, is estimated using the Landy & Szalay (1993) estimator (see also Kerscher, Szapudi & Szalay 2000)

$$\xi(s) = \frac{DD(s)/N_{\text{DD}} - 2DR(s)/N_{\text{DR}} + RR(s)/N_{\text{RR}}}{RR(s)/N_{\text{RR}}}, \quad (4)$$

where  $DD(s)$ ,  $DR(s)$  and  $RR(s)$  are the data–data, data–random, and random–random pair counts at  $s$  for a given bin size  $\Delta s = 10h^{-1}$  Mpc, and  $N_{\text{DD}}$ ,  $N_{\text{DR}}$  and  $N_{\text{RR}}$  are the total numbers of pairs. “Data” refers to observed LRGs. “Random” refers to a randomly resampled subset of a simulated catalogue that mimics the selection effects of the real survey on the sky (boundaries and holes) and in the radial direction under the assumption that the intrinsic galaxy distribution is uniform in comoving space (Kazin et al. 2010, App. A).

Here we use both data and random catalogues from Kazin et al. (2010) (see Sect. 2.1). As in Kazin et al. (2010, App. A), we use radial weights designed to optimise the signal at

about  $100h^{-1}$  Mpc (Feldman, Kaiser & Peacock 1994), as provided in the catalogues, for both the data and random catalogues, and the fibre collision weight is used for angular weighting in the data catalogue. Incompleteness is modelled by sampling the random catalogue with a probability of success equal to the incompleteness estimate for each simulated galaxy. The random catalogues have about 50 times as many galaxies as the data catalogues. In practice in this work, the ratio of the requested number of random galaxies (prior to exclusion of some objects due to incompleteness) to the number of data galaxies,  $N_R^0/N_D$ , has to be several times smaller than 50 in order to achieve realistic computing times. This ratio is specified per individual calculation below. Higher ratios reduce the contribution of Poisson noise to the estimates of  $\xi$ .

### 2.3 Overlap-dependent correlation functions

In order to determine the compression or stretching of comoving features in the correlation function, we consider the subset of LRG pairs that pass “close” to superclusters or voids, respectively. For a given LRG pair, “close” is defined by considering the geometrical overlap  $\omega$  between the object and the pair, where the former is assumed to be the interior of a 2-sphere and the latter a line segment, within flat FLRW comoving space. Figure 1 shows a galaxy–galaxy pair close to a supercluster (or void). In this particular case, the overlap is the chord length, i.e.

$$\omega = 2R \sin \theta. \quad (5)$$

The overlap  $\omega$  is zero when the impact factor is big, i.e. when  $\|\mathbf{e}\| > R$ , where  $\mathbf{e}$  is the normal from the LRG–LRG separation vector to the supercluster (void) centre (see Fig. 1). The most general case is given by

$$\begin{aligned} \omega &= \omega_a + \omega_b \text{ where} \\ \omega_a &= \begin{cases} \min(R \sin \theta, c_a) & \text{if } c_a > 0 \\ \max(-R \sin \theta, c_a) & \text{if } c_a < 0 \\ 0 & \text{if } c_a = 0 \end{cases} \\ \omega_b &= \begin{cases} \min(R \sin \theta, c_b) & \text{if } c_b > 0 \\ \max(-R \sin \theta, c_b) & \text{if } c_b < 0 \\ 0 & \text{if } c_b = 0, \end{cases} \end{aligned} \quad (6)$$

where

$$\begin{aligned} \hat{\mathbf{c}} &:= \frac{\mathbf{c}}{\|\mathbf{c}\|}, \quad c_a := \vec{\mathbf{AS}} \cdot \hat{\mathbf{c}}, \quad c_b := -\vec{\mathbf{BS}} \cdot \hat{\mathbf{c}} \\ \mathbf{d} &:= c_a \hat{\mathbf{c}}, \quad \mathbf{e} := \vec{\mathbf{AS}} + \mathbf{d}. \end{aligned} \quad (7)$$

The simple case illustrated in Fig. 1 and given by Eq. (5) occurs when  $c_a > R \sin \theta > 0$  and  $c_b > R \sin \theta > 0$ .

For any given LRG pair, the overlap with each of the superclusters (or voids) is calculated until either an overlap with  $\omega \geq 1 h^{-1}$  Mpc is found or until all overlaps  $\omega$  have been calculated. An overlap is considered to occur in the former case and not in the latter. For the calculation of  $\xi$ , the maximum value of  $\omega$  for a given LRG pair is forgotten once a decision has been made regarding the existence of an overlap for that pair.

For collecting overlap statistics (Sect. 4.1, Table 4), the calculation of overlaps continues without stopping at the  $\omega < 1 h^{-1}$  Mpc limit. This leads to much longer calculation times, and high memory usage for the calculation of quantiles. This calculation mode is not used for the main calculations (of  $\xi$ ).

The expected differences between comoving correlation function features in rigid comoving space versus inhomogeneous comoving space are likely to depend on whether the pairs are mostly

radial or mostly tangential with respect to the observer. First, let us ignore peculiar velocity effects (“redshift-space distortion”, RSD, e.g. Ballinger et al. 1996). A compression or stretching for superclusters or voids, respectively, can reasonably be expected in either the radial or tangential direction in proportion to the ratio between the locally averaged scale factor and the (large-scale) mean effective scale factor  $a_{\text{eff}}$ . In the tangential direction, a competing effect should be expected from curvature. For example, positive curvature would tend to act as a non-perturbative gravitational lens, so that the would-be compressed BAO peak position is expanded. However, given the estimated parameters of the template metric presented in Roukema et al. (2013), the non-perturbative lensing effect would most likely be weaker than the compression or stretching.

Peculiar velocity effects (Kaiser 1987) complicate analysis of radial separations. The BAO peak is likely to be more difficult to detect in the radial direction.

Thus, we first divide pairs into whether or not they satisfy the criterion  $\omega \geq 1 h^{-1}$  Mpc, and secondly subdivide them according to whether the LRG pair vector is closer to the line-of-sight or rather closer to the sky plane, separating the two cases at  $45^\circ$  using FLRW comoving space geometry. The overlap analysis is carried out independently for DD( $s$ ), DR( $s$ ), and RR( $s$ ) pairs. The Landy & Szalay (1993) estimator, Eq. (4), is used to estimate  $\xi$  separately for each of these components, giving  $\xi_{\parallel}^{\text{sc}}$  and  $\xi_{\perp}^{\text{sc}}$ , for the radial and tangential overlapping components of the correlation function for superclusters, and  $\xi_{\parallel}^{\text{non-sc}}$  and  $\xi_{\perp}^{\text{non-sc}}$ , for the radial and tangential non-overlapping components, and similarly  $\xi_{\parallel}^{\text{void}}$ ,  $\xi_{\perp}^{\text{void}}$ ,  $\xi_{\parallel}^{\text{non-void}}$ ,  $\xi_{\perp}^{\text{non-void}}$ , for voids, respectively.

### 2.4 BAO peak locations

Since the aim of this work is to introduce a new observational method of distinguishing the homogeneous and inhomogeneous assumptions for the comoving metric, we use simple methods that are conservative in the sense that they are more likely to underestimate the shift in the BAO peak location rather than overestimate it, and that we prefer to risk overestimating the error rather than underestimating it.

Thus we use bootstraps (Efron 1979; see also Barrow et al. 1984) which tend to imply overestimates of per-bin correlation function variances rather than underestimates (e.g. Snethlage 1999). Both the random set of LRGs and the list of superclusters (or voids) are randomly resampled (allowing repeats) for each bootstrap simulation. The observed LRG set is not resampled, since the aim is to test the dependence of  $\xi$  on the choice of *subset* of the observed LRG pairs. Resampling the supercluster (or void) catalogue enables statistical modelling of the sensitivity of the results to the inclusion or exclusion of individual superclusters or voids, reducing the chance that our main result—the shift in the BAO peak location—could be mostly the effect of statistical outliers resulting from the supercluster- or void-finding algorithms. Resampling the random catalogue ensures that a major component of the uncertainty in estimating the correlation function itself is statistically represented in the set of bootstrapped correlation functions. The correlation function is calculated separately for each bootstrap resampling. For illustrative purposes only, the standard deviation at each separation  $s$  for the  $N_{\text{boot}}$  bootstraps of a given choice of LRG sample and supercluster or void catalogue is calculated and shown as error bars in plots of  $\xi$ .

Although we expect DD( $s$ ) to shift by  $\Delta s \sim$  a few Mpc in the scalar averaging case, to shift RR( $s$ ) by the same amount would

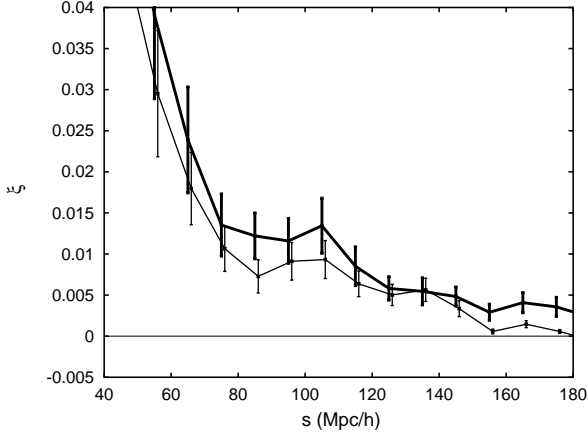


**Figure 2.** Two-point auto-correlation function  $\xi(s)$  for the “bright” (upper curve) and “dim” (lower curve; horizontally offset by  $+1h^{-1}$  Mpc for clarity) samples of luminous red galaxies (LRGs) in the SDSS DR7, as provided by Kazin et al. (2010), against separation  $s$  in  $h^{-1}$  Mpc, assuming an effective metric approximated by an FLRW model with  $(\Omega_{m0} = 0.32, \Omega_{\Lambda 0} = 0.68)$ . The error bars show standard deviations of bootstrapped samples at each given separation  $s$ ; these error bars provide a rough upper limit to the uncertainty and are not used for the analysis. In each case, the ratio  $N_R^0/N_D$  is 16 and the number of bootstraps is 16. The BAO peak at  $\sim 105h^{-1}$  Mpc is sharp for the bright sample and blunt for the dim sample.

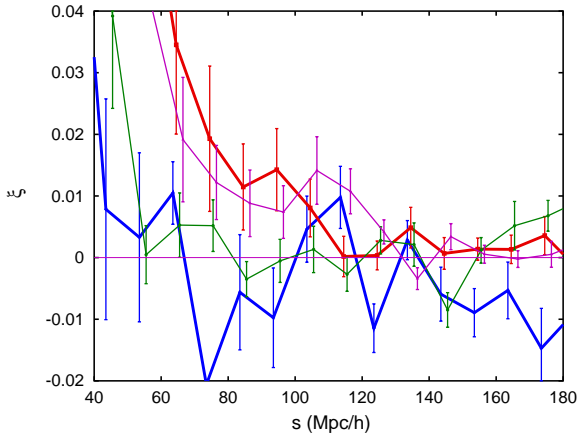


**Figure 3.** Two-point auto-correlation function  $\xi(s)$  for the SDSS DR7 “bright” sample assuming an effective metric approximated by an FLRW model with  $(\Omega_{m0} = 0.32, \Omega_{\Lambda 0} = 0.68)$ , subdivided into radial (blue, lower, thick curve) and tangential (red, upper, thick curve) components overlapping with Nadathur & Hotchkiss (2014) superclusters, and non-overlapping radial (green, lower, thin curve) and tangential (purple, upper, thin curve) components. For clarity, the four curves are offset horizontally by  $-1.5, -0.5, 0.5, 1.5h^{-1}$  Mpc, respectively. The ratio  $N_R^0/N_D = 32, N_{boot} = 8$ . The vertical scale differs from that in Fig. 2. As in Fig. 2, this figure and the following show per-separation-bin bootstrap standard deviations as error bars, providing a rough upper limit guide to the uncertainty, but these are not used for statistical analysis.

be difficult, especially given that we are trying to determine the shift which has so far only been predicted (in this work) qualitatively. The third type of pair count,  $DR(s)$ , would also be difficult to model. Thus, we use the random catalogues without modification, and do not expect a shift of  $\xi$  as simple as  $\xi'(s) = \xi(s + \Delta s)$ . In other words, calculating  $DD(s'), DR(s')$  and  $RR(s')$ , where  $s'$  is

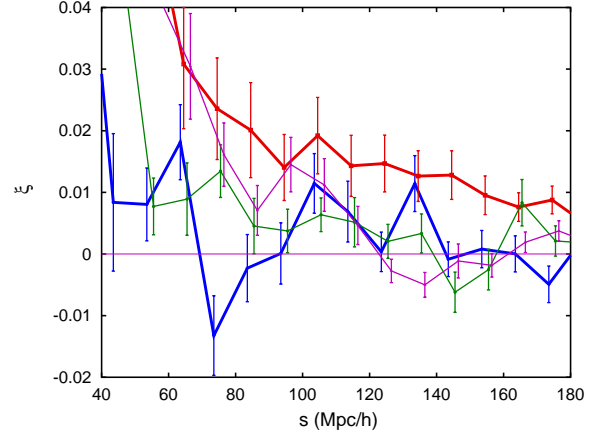


**Figure 4.** As for Fig. 3, for voids, i.e.  $\xi(s)$  for pairs overlapping (radial: blue, lower, thick curve; tangential: red, upper, thick curve) or not overlapping (radial: green, lower, thin curve; tangential: purple, upper, thin curve) with Nadathur & Hotchkiss (2014) voids. The ratio  $N_R^0/N_D = 32, N_{boot} = 8$ .

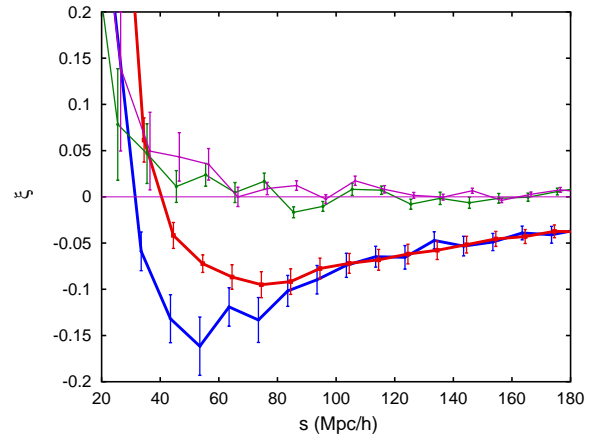


**Figure 5.** As for Fig. 3, for Liivamägi et al. (2012)’s superclusters, i.e.  $\xi(s)$  for pairs overlapping (radial: blue, lower, thick curve; tangential: red, upper, thick curve) or not overlapping (radial: green, lower, thin curve; tangential: purple, upper, thin curve) superclusters. The vertical scale covers a range of about an order of magnitude greater than in the previous plots. The calculation parameters are  $N_R^0/N_D = 16, N_{boot} = 16$ . The integral constraint (not corrected for) obviously has a strong effect for the overlapping components (thick curves).

a Lagrangian separation, in order to infer  $\xi(s')$ , would not be easy. Instead, there is likely to be a general (smooth) change in shape. Since  $RR$  should be a more or less smooth function, the BAO peak should still be visible as a peak above the smooth “background” of the dominant component of  $\xi$ .

To separate the BAO peak from the main part of  $\xi$ , we fit a cubic  $\xi_3$  to the smooth part of  $\xi$  surrounding the peak, i.e. in the range  $40 \leq s \leq 180h^{-1}$  Mpc, excluding  $70 \leq s \leq 130h^{-1}$  Mpc. A linear or quadratic fit would be very sensitive to the choice of  $s$  range for fitting; a higher order polynomial than a cubic could fit part of the peak, effectively weakening it. We subtract the cubic fit, obtaining  $\xi - \xi_3$ , and find the nonlinear least squares best-fit Gaussian for the six  $10h^{-1}$  Mpc bins in the range  $70 \leq s \leq 130h^{-1}$  Mpc, using the Levenberg–Marquardt algorithm (Levenberg 1944; Marquardt

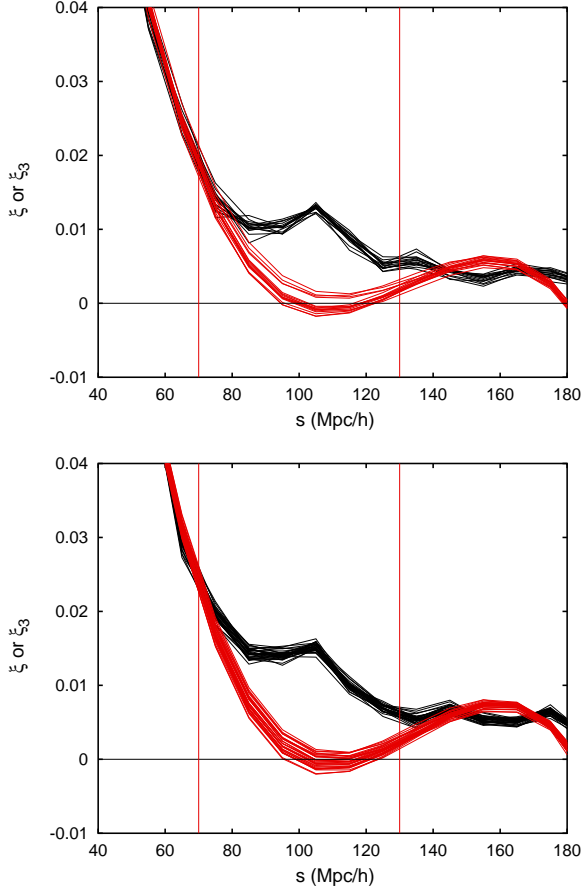


**Figure 6.** Bootstraps estimates  $\xi(s)$  (black online) for the full (“bright”) LRG sample (with no supercluster or void dependence) and best-fit cubics (red online), as described in Sect. 2.4. Vertical lines show the range ( $s < 70$ )  $\cup$  ( $130 < s$ ) (with  $s$  in  $h^{-1}$  Mpc) over which the cubics are fit. Subtracting the cubics (Fig. 7) accentuates the BAO peak. *Upper panel:* pairs in both directions; *lower panel:* tangential pairs.

1963) implemented in LEASQR of the optional OCTAVE packet OCTAVE-OPTIM. Our template Gaussian is centred at  $p_1$ , has width  $p_2$ , height  $p_3$ , and a vertical offset  $p_4$ , i.e.

$$g(x) = p_4 + \sqrt{2\pi} p_3 p_2 G(x, p_1, p_2), \quad (8)$$

where  $G(x, p_1, p_2)$  is a normal probability density function of mean  $p_1$  and standard deviation  $p_2$ . The initial parameter guess is

$$\begin{aligned} p_1 &= 100h^{-1} \text{ Mpc} \\ p_2 &= 5h^{-1} \text{ Mpc} \\ p_3 &= \max_{70h^{-1} \text{ Mpc} \leq s \leq 130h^{-1} \text{ Mpc}} \{\xi - \xi_3\} - p_4 \\ p_4 &= \min_{70h^{-1} \text{ Mpc} \leq s \leq 130h^{-1} \text{ Mpc}} \{\xi - \xi_3\}. \end{aligned} \quad (9)$$

A weighting of  $(1, 2, 4, 4, 2, 1)^6$  for the six bins, respectively, is applied in order to reduce the influence of the tails of the peak, at the risk of biasing the method towards finding the BAO peak location

<sup>6</sup> The convention for this implementation of the Levenberg–Marquardt algorithm is that these should normally correspond to inverse standard deviations per bin; thus, our weighting gives low statistical weight to the tails of the BAO peak and high statistical weight to a fixed BAO peak location independent of the choice of subsample.

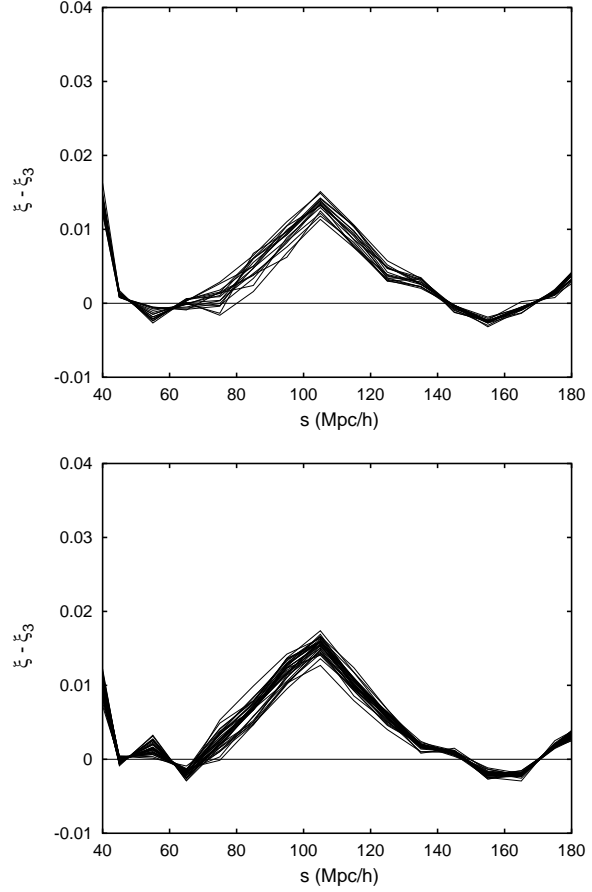


**Figure 7.** Cubic-subtracted two-point auto-correlation function  $\xi(s) - \xi_3(s)$  for the bootstraps of the full (“bright”) LRG sample, corresponding to the subtraction of the respective curves in Fig. 6. *Upper panel:* pairs in both directions; *lower panel:* tangential pairs.

at the same position in all cases. Since this is a bias towards underestimating the true shift, this should give conservative results. We allow up to 30 iterations to find a fit. The centre of the Gaussian,  $p_1$ , is considered to be the estimate  $r$  of the BAO peak location.

While a Gaussian fit to the possibly shifted BAO peak is a reasonable approach for this initial work, there is no need to assume that the errors in the fit themselves follow a Gaussian distribution. Since we have  $N_{\text{boot}}$  bootstrap estimates of the function  $\xi$  in any given case, we calculate the shift of the BAO peak location between a pair of cases  $r', r''$ , by using the sets of BAO peak locations for the bootstraps as discretised estimates of their probability density functions. This avoids assumptions about the shapes of the probability distributions of the two estimates. That is, for each estimate of  $r_{\perp}^0 - r_{\perp}^{\text{sc}}, r_{\perp}^0 - r_{\perp}^{\text{void}}, r_{\perp}^{\text{non-sc}} - r_{\perp}^{\text{sc}},$  or  $r_{\perp}^{\text{non-void}} - r_{\perp}^{\text{void}},$  we take  $r'$  and  $r''$  from bootstrap realisations for the two cases, respectively. Non-convergent BAO peak location estimates are ignored and noted in the table of results. For the estimates of  $r_{\perp}^{\text{non-sc}} - r_{\perp}^{\text{sc}}$  and  $r_{\perp}^{\text{non-void}} - r_{\perp}^{\text{void}},$  the two estimates in a pair come from the same bootstrap realisation. Due to long calculation times,  $N_{\text{boot}}$  for the Liivmägi et al. (2012) case is less than  $N_{\text{boot}}$  for the full sample (without supercluster overlap detection), so half of the full sample realisations are ignored for  $r_{\perp}^0 - r_{\perp}^{\text{sc}}$  in this case. We use robust statistics of this set of realisations to estimate the shift, i.e. we calculate the median  $\mu(r' - r'')$  and we use 1.4826 times the median absolute deviation (Hampel 1974) as an estimate of the standard

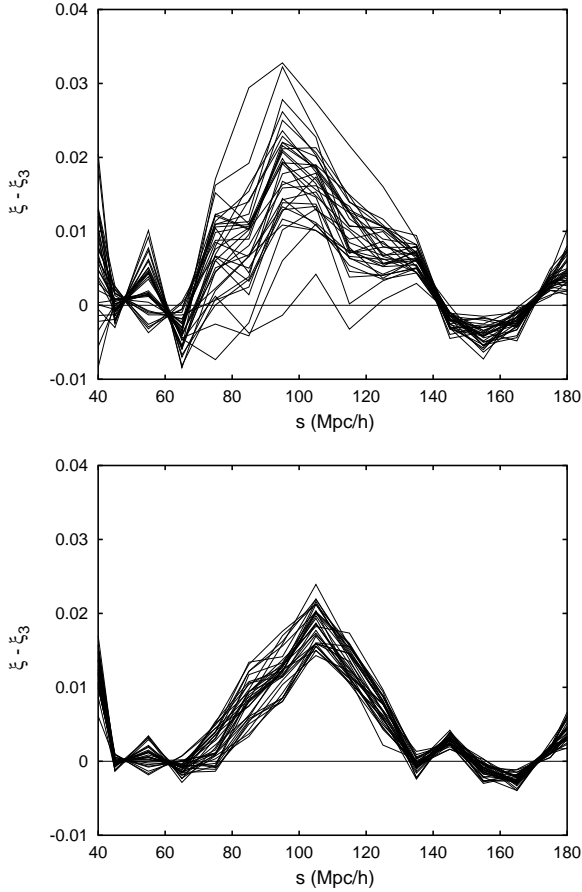


**Figure 8.** Cubic-subtracted two-point auto-correlation function  $\xi(s) - \xi_3(s)$  for the bootstraps for tangential (“bright” sample) LRG–LRG pairs near the Nadathur & Hotchkiss (2014) superclusters (*above*) and for the complementary set of pairs (*below*).

deviation  $\sigma(r' - r'')$ . (Thus, we do not use variances per bin from the bootstraps, nor do we assume Gaussian error distributions in the estimates of the peak locations.)

## 2.5 Optimisation of calculation speed

The calculation time of the two-point auto-correlation functions is dominated by  $N_R^2$ , but is also roughly proportional to the number  $N^{\text{SC}}$  of superclusters or voids. Thus, it scales as  $N_R^2 N^{\text{SC}}$ , requiring many cpu hours of computation. Optimisations used in the present work include:

- (i) while counting pairs in parallel (OPENMP) threads, store the binned pair counts per outer-loop galaxy (the outer loop is parallelised) and only sum these (per separation bin) after the threads have finished; this requires a modest amount of extra memory but favours speed by avoiding atomic/critical instructions;
- (ii) for a given galaxy–galaxy pair, stop calculating overlaps with superclusters or voids if an overlap greater than the threshold ( $1h^{-1}$  Mpc in this work) has already been found (as stated above);
- (iii) inline the vector-related functions and the function to calculate overlap, Eq. (6), by their inclusion in the same file as that for pair count functions and using the gcc compile-time optimisation option -O3.

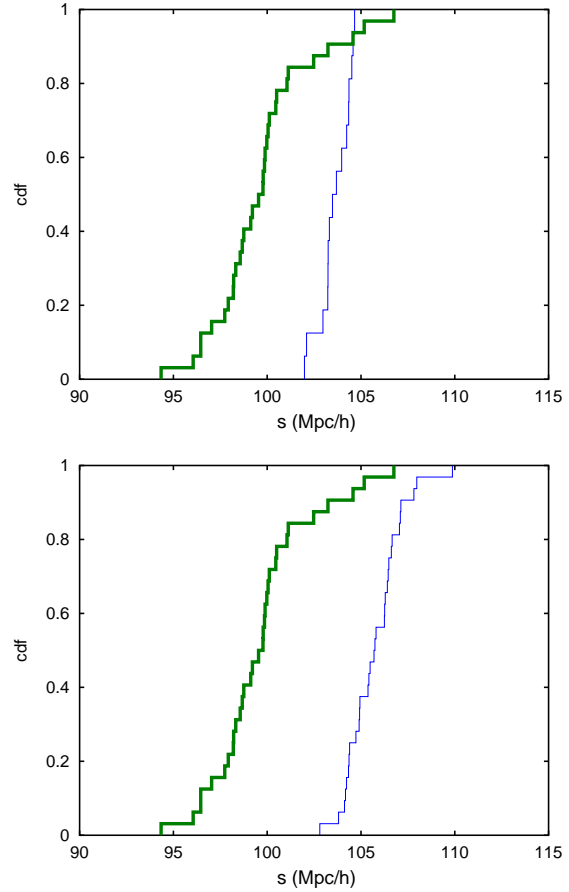


**Figure 9.** Cumulative distribution function (cdf) of Gaussian fit BAO peak locations [Sect. 2.4;  $p_1$  in Eq. (8)] for the bootstraps for tangential (“bright” sample) LRG–LRG pairs near the Nadathur & Hotchkiss (2014) superclusters, shown as a thick (green online) curve in both panels. *Upper panel:* the cdf for bootstrap BAO peak locations for the tangential (“bright”) sample without overlap selection is shown as a thin (blue online) curve; *lower panel:* the cdf for the complementary set of pairs (those not overlapping with superclusters) is shown as a thin (blue online) curve. The lower panel corresponds to the two panels of Fig. 8.

Significant speedup for flat space calculations might also be possible using a *kd* tree approach (e.g. Moore et al. 2001).

## 3 RESULTS

Figure 2 shows a sharp BAO peak for the bright sample and a broad, less well-defined peak for the dim sample. Thus, we analyse the former. The calculations described below, i.e. for the bright sample, made using the optimisations described in Sect. 2.5, represent about 240,000 cpu-core-hours of computation on Intel Xeon E7-8837 processors.

The correlation functions for tangential pairs either overlapping or not overlapping with Nadathur & Hotchkiss (2014) superclusters or voids are shown as the two upper curves (red, purple online) in Figs 3 and 4. Keeping in mind that the per-bin standard deviation (estimated from bootstraps as shown or by other methods) does not directly show the uncertainty in the existence or position of the BAO peak, the best estimate of  $\xi$  does appear to be present for all four of these curves in the separation bins centred at



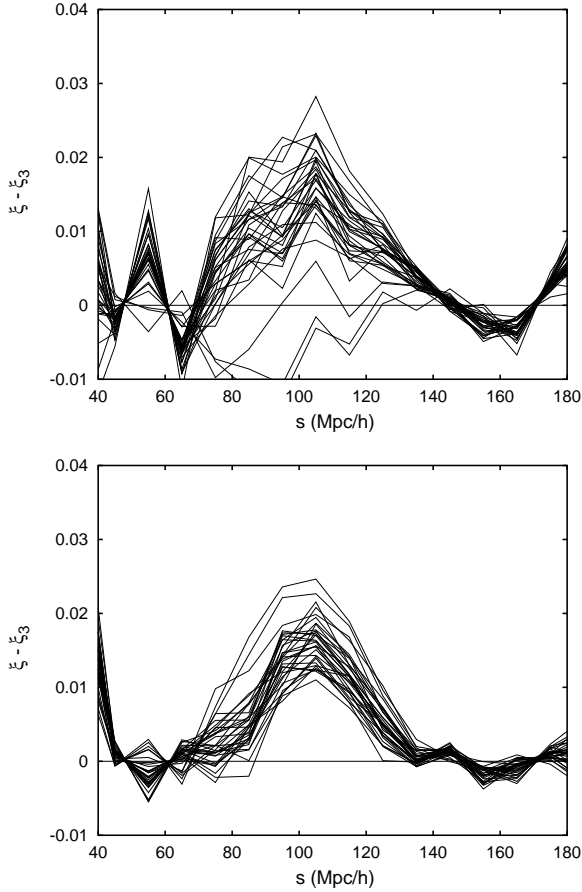


**Figure 10.** Cubic-subtracted two-point auto-correlation function  $\xi(s) - \xi_3(s)$  for the bootstraps for tangential (“bright” sample) LRG–LRG pairs near the Nadathur & Hotchkiss (2014) voids (*above*) and for the complementary set of pairs (*below*).

either  $95h^{-1}$  Mpc or  $105h^{-1}$  Mpc. For overlaps with superclusters or for LRG pairs not overlapping with voids the peak appears to be located at  $95h^{-1}$  Mpc. For overlaps with voids or for non-overlaps with superclusters, the BAO peak appears to be at  $105h^{-1}$  Mpc, i.e. at the same location as that of the full sample.

The correlation functions for radial pairs either overlapping or not overlapping with Nadathur & Hotchkiss (2014) superclusters or voids are shown as the two lower curves (blue, green online) in Figs 3 and 4. Clearly, the Kaiser effect (large-scale smooth infall Kaiser 1987) significantly affects  $\xi$  on these scales. Moreover, since we define the split between radial and tangential pairs at an angle of  $45^\circ$  with respect to the plane of the sky, there are many fewer radial than tangential pairs (the sky plane is two-dimensional). Thus, use of the radial case for detecting a shift in the BAO peak location would risk ambiguity in identifying the peak and most likely be subject to higher systematic error than the tangential case. The radial curves are not used further in the present work.

The Liivamägi et al. (2012) supercluster correlation functions are shown in Fig. 5. There is a great difference between the tangential and radial supercluster-overlapping functions, and a very strong difference between these and the non-supercluster-overlapping pair correlation functions. This is easily interpreted as an effect of the integral constraint (see, e.g., Fig. 7, lower panel, Roukema & Peterson 1994), for which we have not made any corrections, since our aim is to detect the shift in the BAO peak loca-

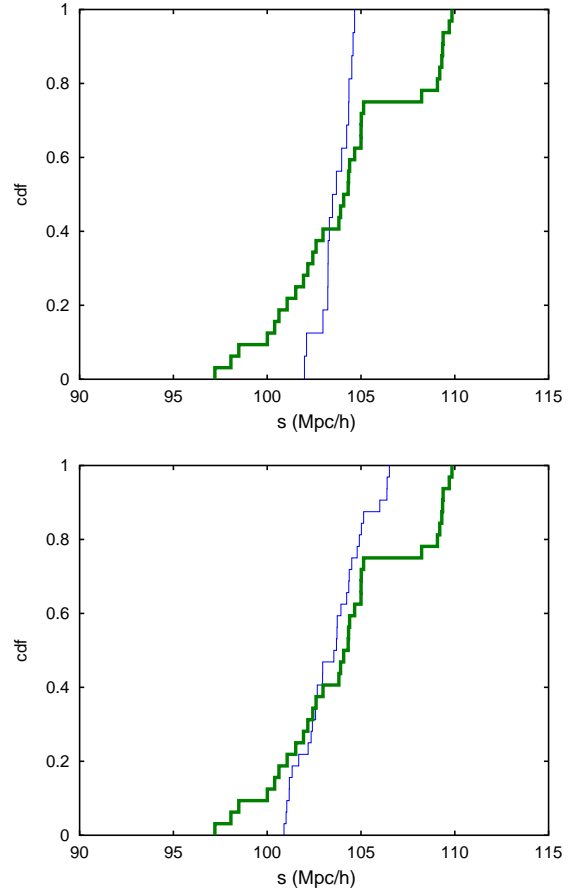


**Figure 11.** As for Fig. 9, cdf of BAO peak locations for tangential LRG–LRG pairs near the Nadathur & Hotchkiss (2014) voids, shown as a thick (green online) curve in both plots, compared to that for the tangential sample without selection (thin curve, blue online, upper plot) and to that for pairs that do not overlap with voids (thin curve, blue online, lower plot). The lower panel corresponds to the two panels of Fig. 10.

tion rather than attempting to model the general change in the shape of the correlation function. A BAO peak for the Liivamägi et al. (2012) tangential supercluster-overlapping case (red thick curve) is barely visible by inspection of Fig. 5. In the non-supercluster-overlapping case, a BAO peak is obvious in the  $100\text{--}110h^{-1}$  Mpc bin, but a broad weaker peak with maxima in the  $70\text{--}80h^{-1}$  Mpc and  $80\text{--}90h^{-1}$  Mpc bins suggests that the detection is ambiguous. However, we retain the method defined above (Sect. 2.4), without any modification, in order to examine these two curves, i.e. for each of the bootstrap estimates of these correlation functions, we subtract a best-fit cubic and least-squares fit a gaussian in order to estimate the BAO peak location. As shown below, subtracting best-fit cubics yields clear BAO peaks in both cases.

Cubic fits for individual bootstrap correlation functions, as described in Sect. 2.4, are shown in Fig. 6. Clearly, the amplitude of the BAO peak after subtracting the cubic would differ significantly from that obtained from fitting a smooth function with a narrower exclusion region around the peak. Since the aim here is to measure the shift in the peak location, not the peak’s amplitude, this should not affect our results. Cubic-subtracted bootstrap correlation functions are shown in Figs. 7, 8, 10, and 12, for the full sample and for the tangential LRG pairs. The BAO peak is clearly visible in



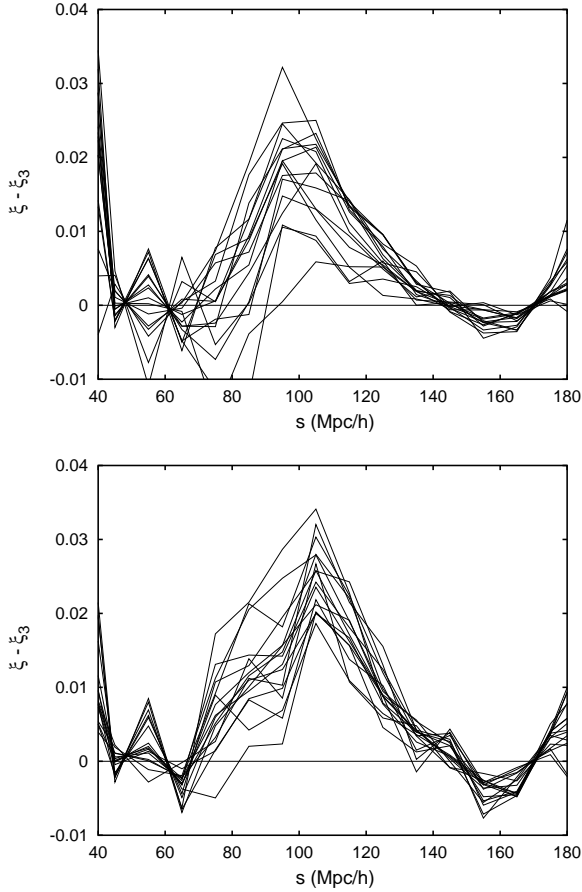


**Figure 12.** Cubic-subtracted two-point auto-correlation function  $\xi(s) - \xi_3(s)$  for the bootstraps for tangential (“bright” sample) LRG–LRG pairs near the Liivamägi et al. (2012) superclusters (*above*) and for the complementary set of pairs (*below*). Since this shows the cubic-subtracted correlation function, the vertical scale is identical to that of Figs 7, 8 and 10, in contrast to Fig. 5, which has a different vertical scale to those of Figs 2, 3 and 4. In comparison to Fig. 5, per-bin variance is reduced, because cubic-subtraction removes much of the noise introduced by the per-bootstrap integral constraint.

all of these plots, although some of the correlation functions for individual bootstraps fail to show it clearly.

The upper panels of Figs 8 and 12, i.e. for LRG–LRG pairs overlapping superclusters, clearly show that most (Nadathur & Hotchkiss 2014) or many (Liivamägi et al. 2012) of the bootstrapped correlation function BAO peaks are centred in the  $90\text{--}100h^{-1}$  Mpc bin. In contrast, the lower panels of these two figures show similar behaviour to Fig. 7: the BAO peak is centred in the  $100\text{--}110h^{-1}$  Mpc bin. The lower panel of Fig. 10, for LRG–LRG pairs not overlapping with voids, shows a weaker compression; a minority of the bootstrap correlation functions have a BAO peak centre in the  $90\text{--}100h^{-1}$  Mpc bin.

Fitting Gaussians to these bootstrapped BAO peaks yields estimates of the BAO peak locations. The cumulative distribution functions (cdf’s) of these estimates are shown in Figs. 9, 11, and 13. It is obvious that the pairs of cdf’s are incompatible in both Figs. 9 and 13, i.e. when the supercluster-overlapping BAO peak location is compared to either the full sample BAO peak location or the complementary-pair BAO peak location. The Kolmogorov–Smirnov two-sided probabilities that the two members of a pair of

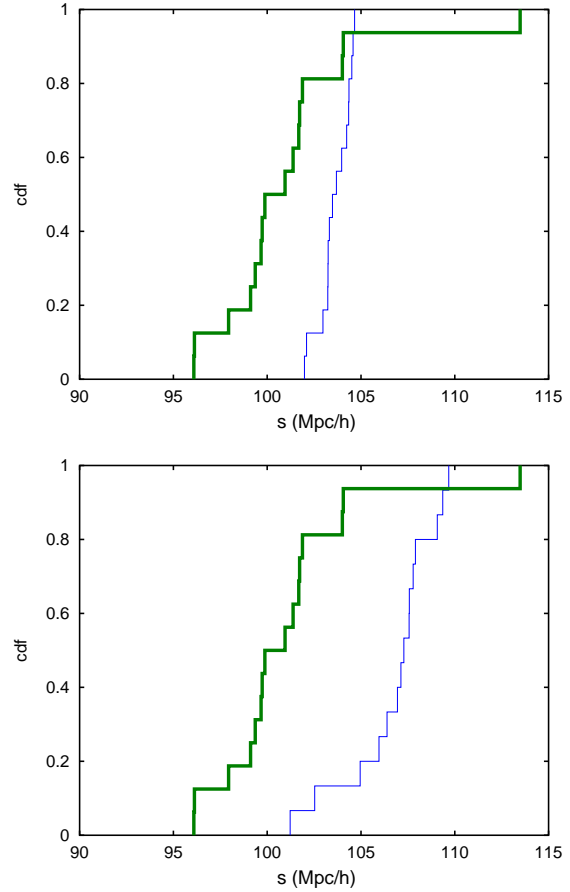


**Figure 13.** As for Fig. 9, cdf of BAO peak locations for tangential LRG–LRG pairs near the Liivamägi et al. (2012) superclusters, shown as a thick (green online) curve in both plots, compared to that for the tangential full sample (thin curve, blue online, upper plot) and to that for pairs that do not overlap with superclusters (thin curve, blue online, lower plot). The lower panel corresponds to the two panels of Fig. 12.

**Table 2.** Kolmogorov–Smirnov probabilities of identical cumulative distribution functions

catalogue	$r_{\perp}^0, r_{\perp}^{\text{sc}}$	$r_{\perp}^{\text{non-sc}}, r_{\perp}^{\text{sc}}$	$r_{\perp}^0, r_{\perp}^{\text{void}}$	$r_{\perp}^{\text{non-void}}, r_{\perp}^{\text{void}}$
N&H <sup>a</sup>	$3 \times 10^{-10}$	$5 \times 10^{-11}$ <sup>b</sup>	0.05	0.3 <sup>c</sup>
LTS <sup>d</sup>	$5 \times 10^{-5}$	$3 \times 10^{-5}$ <sup>e</sup>		

<sup>a</sup>Nadathur & Hotchkiss (2014).

<sup>b</sup>Columns 1, 2 correspond to Fig. 9.

<sup>c</sup>Columns 3, 4 correspond to Fig. 11.

<sup>d</sup>Liivamägi et al. (2012).

<sup>e</sup>Columns 1, 2 correspond to Fig. 13.

cdf’s represent samples drawn from a single continuous underlying distribution are listed in Table 2. For the supercluster-overlapping comparisons (first and second columns of Table 2), identity of the distributions is rejected to very high significance (greater than 99.99%).

The probabilities in Table 2 are not sufficient to show that the differences in distributions constitute shifts in the BAO peak location rather than, for example, differences in noise levels, i.e. widths

**Table 3.** Compression<sup>a</sup> of BAO peak location in  $h^{-1}$  Mpc

catalogue	$r_{\perp}^0 - r_{\perp}^{\text{sc}}$	$r_{\perp}^{\text{non-sc}} - r_{\perp}^{\text{sc}}$	$r_{\perp}^0 - r_{\perp}^{\text{void}}$	$r_{\perp}^{\text{non-void}} - r_{\perp}^{\text{void}}$
N&H <sup>b</sup>	$4.3 \pm 1.6$	$6.6 \pm 2.8^c$	$-0.2 \pm 4.0$	$-1.1 \pm 5.5^{d,e}$
LTS <sup>f</sup>	$3.7 \pm 2.9$	$6.3 \pm 2.6^{g,h}$		

<sup>a</sup>A positive (negative) value in columns 1 or 3 indicates compression (stretching) compared to the full sample BAO peak location. A positive (negative) value in columns 2 (4) indicates compression (stretching) of the BAO peak location for overdensity-selected (underdensity-selected) pairs compared to the complementary set of pairs.

<sup>b</sup>Nadathur & Hotchkiss (2014).

<sup>c</sup>Columns 1, 2:  $N_{\text{R}}^0/N_{\text{D}} = 32$ ,  $N_{\text{boot}} = 32$ .

<sup>d</sup>Columns 3, 4:  $N_{\text{R}}^0/N_{\text{D}} = 32$ ,  $N_{\text{boot}} = 32$ .

<sup>e</sup>Columns 3, 4: The Gaussian BAO peak fit failed for one of the 32 bootstraps and was thus ignored in the estimate of  $r_{\perp}^{\text{void}}$ .

<sup>f</sup>Liivamägi et al. (2012).

<sup>g</sup>Columns 1, 2:  $N_{\text{R}}^0/N_{\text{D}} = 16$ ,  $N_{\text{boot}} = 16$ .

<sup>h</sup>Columns 1, 2: Gaussian BAO peak fits failed for two of the 16 bootstraps and were thus ignored in the estimate of  $r_{\perp}^{\text{sc}}$  for the Liivamägi et al. (2012) superclusters.

**Table 4.** Fraction of LRG–LRG pairs that overlap with superclusters or voids<sup>a</sup>

catalogue	$f_{\text{DD}}$	$f_{\text{DR}}^b$	$f_{\text{RR}}^b$
N&H superclusters <sup>c</sup>	$0.79 \pm 0.24$	$0.76 \pm 0.23$	$0.80 \pm 0.02$
N&H voids <sup>c</sup>	$0.82 \pm 0.19$	$0.60 \pm 0.19$	$0.83 \pm 0.07$
LTS superclusters <sup>d</sup>	$0.95 \pm 0.01$	$0.72 \pm 0.02$	$0.91 \pm 0.01$

<sup>a</sup>Median and 1.4826 times the median absolute deviation (Hampel 1974) of the overlapping fraction for the bootstrap realisations, for the three types of pairs.

<sup>b</sup>This table is calculated for  $N_{\text{R}}^0/N_{\text{D}} = 1$ ; and  $N_{\text{boot}} = 32, 32, 16$ , respectively, for the three cases.

<sup>c</sup>Nadathur & Hotchkiss (2014).

<sup>d</sup>Liivamägi et al. (2012).

rather than central tendencies. The best estimates of the shifts are listed in Table 3.

Table 3 shows that the supercluster-overlapping BAO peak location is about  $6\text{--}7h^{-1}$  Mpc less than that of the complementary set of LRG pairs and about  $4h^{-1}$  Mpc less than that of the full sample of pairs. These shifts are statistically significant at about the  $2.5\sigma$  level (in terms of Gaussian intuition) for the Nadathur & Hotchkiss (2014) superclusters, and at weaker significance for the Liivamägi et al. (2012) superclusters.

## 4 DISCUSSION

Figures 7–9, 12, and 13, and Tables 2 and 3 clearly show that the supercluster-overlapping BAO peak location for tangential pairs is about  $6\text{--}7h^{-1}$  Mpc less than that for the non-supercluster-overlapping pairs, i.e. superclusters correspond to a compression of about 6%. A weaker compression is found in comparison to the full-sample tangential pairs, i.e. without overlap selection. The best estimates of the shift in the void-overlapping case are much smaller, as expected for a void-dominated best-fit metric, though with high uncertainties. This trend of strong relative compression of the supercluster-overlapping BAO peak location and a weak

stretching in the void-overlapping case qualitatively agrees with what is expected for inhomogeneous models. Analysis of other surveys should reduce the statistical uncertainties to see if the trend continues to favour an inhomogeneous metric.

Theoretical interpretation of these results will require taking into account the typical fraction of a separation path that actually overlaps with a supercluster or void. For separations in the  $70 < s/h^{-1} \text{ Mpc} < 130$  range, the median overlap is about 70, 85, and  $40h^{-1}$  Mpc for the Nadathur & Hotchkiss (2014) superclusters, voids, and Liivamägi et al. (2012) superclusters, respectively, i.e. roughly 70%, 85%, and 40% of the BAO-scale separation paths should be compressed, stretched, and compressed, respectively. We present observational caveats within the FLRW (rigid comoving) interpretation of the data in Sect. 4.1. In Sect. 4.2, we propose a method of more accurate analysis by using an effective template metric rather than the  $\Lambda$ CDM metric for the assumed cosmological model. In Sect. 4.3, we discuss possible relations of the present work to other well-known dark-energy-free general-relativistic approaches to cosmology. We focus on observational methods or claims of detecting metric inhomogeneity in Sect. 4.4. In Sect. 4.5, we list some observational results that reject the  $\Lambda$ CDM model.

### 4.1 Observational caveats and improvements

Could the superclusters listed by Nadathur & Hotchkiss (2014) and Liivamägi et al. (2012) constitute very rare overdensity fluctuations, so that the LRG pairs that overlap them (given our definition in Sect. 2.3) constitute a strongly biased subset that favours rare, highly nonlinear  $100h^{-1}$  Mpc fluctuations? Table 4 shows that on the contrary, the overlapping pair fractions are high, about 80–90%. The numbers of superclusters vary by a factor of 10 between the two groups’ analyses (Table 1), but in neither case can the compressed BAO scale be attributed to the rarity of the superclusters and associated LRG–LRG pairs.

Our result could be thought of in terms of a “non-random” jackknife type analysis of the set of  $\sim 10^9$  SDSS DR7 “bright” LRG–LRG pairs. Given that the full set of  $\sim 10^9$  pairs gives the standard BAO peak location, how easy is it to choose about 10–20% of these pairs to ignore so that the BAO peak location of the remainder is reduced by about  $6h^{-1}$  Mpc? We know one answer (for the tangential pairs): choose either the Nadathur & Hotchkiss (2014) or Liivamägi et al. (2012) supercluster catalogue, and ignore those pairs that do not overlap these superclusters by  $1h^{-1}$  Mpc or more. Only a minority of pairs are excluded, and the BAO peak standard ruler is compressed by about  $6h^{-1}$  Mpc. Our result would be difficult to explain as a bias towards very rare fluctuations.

Could strong or weak gravitational lensing create a bias that has been ignored here? Gravitational lensing, in the sense of observations interpreted by perturbative calculations against an FLRW background, does not imply large offsets in path lengths projected to a comoving spatial slice. For example, multiply imaged galaxies have time delays ranging from a few days to a few years (e.g. Table 2 Paraficz & Hjorth 2010), i.e. radial paths should vary by sub-parsec scales rather than megaparsec scales. In the tangential direction, strong lensing typically plays a role on arcsecond scales, and weak lensing (shear of galaxy images) shows correlations at arcminute scales (e.g. Schneider 2005, and refs therein). These are both much smaller than the degree scales that would need to affect the scale of the BAO peak in tangential directions.

Could peculiar velocity effects be relevant? We chose to use the “tangential” pairs, i.e. those which lie within  $45^\circ$  of the sky plane, so peculiar velocity effects should be weak. Within a  $\Lambda$ CDM

model, a (radial) peculiar velocity of 1000 km/s at  $z = 0.3$  consists of a multiplicative error in  $(1+z)$  of 1.003, corresponding to about  $10h^{-1}$  Mpc. The “finger of God” effect is unlikely to be significant, since we consider separations well above  $10h^{-1}$  Mpc. However, the larger scale Kaiser effect (Kaiser 1987) is of the order of magnitude to potentially be of concern. This has long been expected to have significant effects in the radial direction on redshift-space separation scales of tens of megaparsecs, in the sense of shifting power to smaller scales (e.g. Ballinger et al. 1996; Matsubara & Suto 1996). Recent models and estimates (e.g. Song et al. 2014, and references therein) show considerable differences between the overall shapes of the radial and tangential correlation functions, qualitatively consistent with what is shown in the figures above. Jeong et al. (2014) estimate that the BAO peak location estimated directly from  $\xi$ , without removal of the smooth component of the function, can yield a difference between the exactly radial and tangential directions of about  $3h^{-1}$  Mpc. However, they also estimate (Fig. 6 right, Jeong et al. 2014) that when the smooth component is removed (by two methods different to our choice of subtracting a best-fit cubic), the difference is reduced to about  $0.2\text{--}1.0h^{-1}$  Mpc.

In our analysis, we do not compare exactly radial pairs to exactly tangential pairs; we compare “tangential” samples to each other, defined by a  $45^\circ$  split. Nevertheless, let us consider an extreme case in order to estimate an upper bound to this effect. If one of our “tangential” samples would consist of exactly line-of-sight pairs and the other uniquely of  $45^\circ$  pairs, then the Jeong et al. (2014) analysis for smooth-component-removed BAO peak locations would suggest a difference below their  $0.2\text{--}1.0h^{-1}$  Mpc estimate for exactly tangential versus radial pairs. Our BAO peak location estimation method, which is preceded by the removal of a best-fit cubic, would be likely to give a similar result.

More realistically, any two subsamples that we compare in this work consist of pairs whose angles with respect to the sky plane are distributed between  $0^\circ$  and  $45^\circ$ , not Dirac-delta distributed at one or the other of these. However, the distributions are unlikely to be exactly identical. It is likely that, at least due to the role of Poisson noise, either the median angle to the line-of-sight of the “tangential” pairs that overlap superclusters is slightly greater than the median angle of pairs that do not overlap superclusters, or vice-versa. This angular difference, or the overall distributions of angles with respect to the sky plane, should give a small distortion in our result, but by much less than the  $0.2\text{--}1.0h^{-1}$  Mpc indicated above. Correcting for this would not remove the shift that we have detected for the Nadathur & Hotchkiss (2014) and Liivamägi et al. (2012) catalogues, as given in Table 3, but would be useful to include in future work in order to obtain more results at the sub-megaparsec level.

The present results should be obtainable at higher statistical significance in existing catalogues (e.g., BOSS DR11 LOWZ and CMASS) and future data sets such as those from SDSS-III/BOSS DR12, SDSS-IV/eBOSS, LSST, EUCLID, VISTA/4MOST (de Jong et al. 2012) and DESI (Levi et al. 2013). At lower redshifts than those of SDSS DR7 LRGs ( $z \sim 0.3$ ), the Universe is more inhomogeneous, but there is very little volume to sample well at the  $100h^{-1}$  Mpc scale. At higher redshifts  $z < 1$ , the amount of volume to sample is higher, but the inhomogeneity (virialisation fraction) is lower, so the effect should be weaker. Despite these difficulties, the redshift evolution of the BAO peak location shift for superclusters, i.e. the  $r_{\perp}^{\text{non-sc}} - r_{\perp}^{\text{sc}}$  vs  $z$  relation, should constitute a new statistic that would need to be explained quantitatively in scalar averaging, dark-energy-free models or in  $\Lambda$ CDM or other FLRW models, e.g. with inhomogeneous dark energy. As observa-

tional accuracy improves and theoretical predictions are made, this will provide a geometrical test to distinguish the two.

## 4.2 Improved analysis assuming scalar averaging

The  $\Lambda$ CDM best-fit metric interpretation of the data, which we have used above, uses a distance–redshift relation based on the assumption that the expansion rate of the averaged 3-spatial slices exactly equals that of homogeneous, unaveraged 3-spatial slices. This assumption, of the FLRW models in general, is that the implicitly averaged constant-curvature time slices happen, fortuitously, to evolve in the way that idealised exactly homogeneous slices would evolve. A more realistic interpretation would be possible using a template metric (Larena et al. 2009; Roukema et al. 2013). This would not only help test the validity of the template metrics that have so far been proposed, but should also yield more accurate estimates of the BAO peak location shift.

Theoretical work in inhomogeneous cosmology in general should also be useful not only in making predictions and interpretations, but also in improving the observational analysis. For example, we have assumed that the projection of photon paths from the past time cone to the comoving spatial section does not significantly affect the expected compression or stretching of comoving separations. Since we focus on tangential separations, this seems to be a reasonable assumption, but ray tracing in scalar averaging models or Swiss cheese models (e.g. Futamase & Sasaki 1989; Marra et al. 2007; Szybka 2011; Fleury, Dupuy & Uzan 2013a,b) should be checked, especially for extending the method used here to radial pairs. Changes to the BAO peak location in the radial direction are likely to be more complicated to extract than for tangential pairs, but might contain more useful cosmological information.

## 4.3 Other inhomogeneous approaches

Other dark-energy-free general-relativistic approaches to observational cosmology include Stephani models (Dabrowski & Hendry 1998) and Lemaître–Tolman–Bondi (LTB) solutions. The latter are often applied as a local void model (e.g. Mustapha et al. 1997; Célérier 2000; Tomita 2001; Alnes et al. 2006; Garcia-Bellido & Haugbølle 2008; Enqvist 2008; Alexander et al. 2009; Biswas et al. 2010; Hunt & Sarkar 2010; Bolejko et al. 2011), sometimes infer a local hump from observational data (Célérier, Bolejko & Krasiński 2010; Kolb & Lamb 2009), and are widely used in “Swiss cheese” models (e.g. Biswas & Notari 2008; Bolejko & Célérier 2010; Lavinto et al. 2013, and references therein). LTB models are also used to argue that within homogeneous (FLRW) cosmology for non-evolving dark energy, i.e. a cosmological constant model, the value of the cosmological constant will be mis-estimated by about a percent if non-perturbative calculations are not taken into account (Enea Romano & Chen 2011; Enea Romano et al. 2014). Independently of the kinematic Sunyaev–Zel’dovich effect arguments against the local void model (Moss, Zibin & Scott 2011; Zhang & Stebbins 2011; Zibin & Moss 2011), a local void (or hump) should not have a strong effect on the BAO peak location test introduced here, since our test is differential, comparing different subsamples of a single survey in a given volume of space. However, if the whole survey (e.g. SDSS DR7 LRGs) were contained in a  $1h^{-1}$  Gpc void centred not too far from the Galaxy, then the large-scale gradient in underdensity could probably introduce a small bias, in a similar way in which it would affect estimates of the “full” BAO peak location.

Swiss cheese models typically use an FLRW “background” model for the “cheese” and LTB models for the “holes”. For a given Swiss cheese model, it should be possible to study the differential evolution of pairs of tracer galaxies that overlap cheese versus the complementary set of pairs, or that overlap voids versus the complement. Since most tracers should lie in the “cheese”, their pairs would already be comoving by definition of the model. It should be possible to calculate the pairs’ comoving separations by integration of the (analytically exact) metric of the model. A differential study of the complementary sets of pairs would probably provide the simplest way to model the expected shift in the BAO peak location in this class of inhomogeneous models.

#### 4.4 Observational methods of detecting metric inhomogeneity and claims of detections

Observational methods of distinguishing the literally homogeneous FLRW model from statistically homogeneous relativistic models have mostly focussed on the distance-modulus–redshift relation (to fit supernovae type Ia observations) or estimates of  $H(z)$  versus  $z$ , i.e. the expansion-rate–redshift relation (e.g. Smale & Wiltshire 2011; Boehm & Rasanen 2013). Perturbed FLRW strategies for detecting inhomogeneity also focus on the expansion rate (e.g. Räsänen 2012), and especially its variance (Ben-Dayan et al. 2014). [Redshift drift is a test that distinguishes spherically symmetric inhomogeneous models, the LTB and Stephani models, from each other and from the  $\Lambda$ CDM model (e.g. Balcerzak & Dabrowski 2013).]

While several dark-energy-free inhomogeneous models claim to have fit several sets of extragalactic observations (Sect. 4.3; see also Duley et al. 2013), some focus on tests that are qualitatively new. Fleury et al. (2013a) argue that a single FLRW metric is relativistically inaccurate for modelling both wide-angle observations [cosmic microwave background (CMB), BAO] and narrow-angle observations (type Ia supernovae), and appear to resolve conflicting estimates of  $\Omega_{m0}$  using a Swiss cheese model with FLRW cheese. On scales up to tens of megaparsecs from the Galaxy, Wiltshire et al. (2013) find that galaxy peculiar velocity flow analyses imply a relation between the Local Group rest frame and what is normally considered to be the CMB comoving rest frame that is different from the FLRW expectation. Saulder et al. (2012) propose to analyse the dependence of the expansion rate (Hubble parameter) on line-of-sight environment, i.e. mostly through dense structures versus mostly through voids and present preliminary results.

#### 4.5 Observational methods that reject the $\Lambda$ CDM model

The method presented here is not the only one that potentially or already rejects the  $\Lambda$ CDM model. While many observations agree with the latter, several recent observational results (other than the present work) reject it. An incomplete list includes the following. Flender et al. (2013) find that what is generally accepted as a detection of the integrated Sachs–Wolfe (ISW) effect in the CMB is stronger than the  $\Lambda$ CDM expectation at the  $3\sigma$  level. Wiegand, Buchert & Ostermann (2014) find that Minkowski functional analysis (which implicitly includes all orders of  $n$ -point auto-correlation functions) of the SDSS DR7 significantly rejects the  $\Lambda$ CDM model on scales of several tens of megaparsecs in volume-limited samples of  $500h^{-1}$  Mpc ( $3\sigma$ ) and  $700h^{-1}$  Mpc ( $2\sigma$ ). Earlier Minkowski functional analysis on smaller and sparser catalogues, using the same or complementary methods, had found that the

fluctuations were compatible with  $\Lambda$ CDM mock catalogues (e.g. Kerscher et al. 2001; Hikage et al. 2003). Chuang et al. (Fig. 6, 2013) find that the CMASS and WiggleZ (Blake et al. 2012) normalised growth rate estimates contradict the Planck Surveyor cosmic microwave background  $\Lambda$ CDM model at about  $2\sigma$  significance. By comparing CFHTLenS weak lensing analysis with a parametrisation of the  $\Lambda$ CDM version of the FLRW model using Planck and WMAP data, MacCrann et al. (2014) reject the model at the 90–96% level (but at only the 64% level if a sterile neutrino is included). Battye, Charnock & Moss (2014) reject the  $\Lambda$ CDM model at the  $5\sigma$  level based on contradictions between large-scale and small-scale power, unless the sum of neutrino masses is increased above that of the Planck base model of 0.06 eV (Sect. 6.3.1, Ade et al. 2014). The BAO peak (without any shift measurement) detected in the Lyman  $\alpha$  forest in front of about  $10^5$  quasars at  $z \sim 3$  was estimated to reject the  $\Lambda$ CDM model at the  $2.5\sigma$  level (Delubac et al. 2015). A significant contradiction exists between Galactic metal-poor star estimates of the pre-Galactic  ${}^7\text{Li}$  abundance and the abundance inferred from either primordial big bang nucleosynthesis or the cosmic microwave background interpreted according to an FLRW model (Cyburt et al. 2008), unless new particles such as decaying gravitinos are assumed (e.g. Cyburt et al. 2013).

## 5 CONCLUSION

We have introduced supercluster-overlap dependent BAO peak location estimation as a new observational method of distinguishing the FLRW models (including the  $\Lambda$ CDM model), which assume rigidity of comoving space, from scalar averaging models, which allow comoving space to be curved and compressed or stretched by structure formation. The initial results from the SDSS DR7 are promising, showing that by choosing the sharpest signal, that of “tangential” LRG pairs, a detection of compression in the BAO peak location for supercluster-overlapping pairs versus complementary pairs is significant at about the  $2.5\sigma$  level for two different supercluster catalogues:  $6.6 \pm 2.8h^{-1}$  Mpc for Nadathur & Hotchkiss (2014) superclusters and  $6.3 \pm 2.6h^{-1}$  Mpc for Liivamägi et al. (2012) superclusters. Compression relative to the full (tangential) sample is, as expected, weaker:  $4.3 \pm 1.6h^{-1}$  Mpc and  $3.7 \pm 2.9h^{-1}$  Mpc, respectively. Stretching in the void-overlapping case is numerically consistent with what is expected (negative compression in columns 3 and 4 of Table 3, i.e. stretching), but statistically insignificant. The differences in the bootstrap estimates of the BAO peak locations for supercluster-overlapping pairs versus complementary pairs are strikingly obvious in Fig. 8 and Fig. 9 (lower panel) for the Nadathur & Hotchkiss (2014) superclusters, and in Fig. 12 and Fig. 13 (lower panel) for the Liivamägi et al. (2012) superclusters. The corresponding Kolmogorov–Smirnov formal estimates of incompatibility in the cumulative distribution functions (Table 2) reflect the strength of the differences visible by inspection in these figures.

Qualitatively, these results are consistent with what is expected from scalar averaging and inconsistent with what is expected in the rigid comoving space models, including the  $\Lambda$ CDM model. Theoretical work on the BAO peak location shift in both approaches, together with observational development of the test, may potentially challenge the  $\Lambda$ CDM model and constrain back-reaction models. For example, application of our test to  $\Lambda$ CDM  $N$ -body simulations would provide a check in terms of a widely used tool of FLRW cosmology. This test should be compared

to the expected  $\Lambda$ CDM low-redshift BAO peak location shift of less than 0.3% [Eqs (30), (31), Sherwin & Zaldarriaga 2012; see also McCullagh, Neyrinck, Szapudi & Szalay 2013; and references therein; see also e.g. Slepian & Eisenstein (2015), for baryon–dark-matter relative-velocity corrections] which is much smaller than the environment-dependent shift of 6% which is found here.

## ACKNOWLEDGMENTS

Thank you to Tomasz Kazimierzczak, Hirokazu Fujii, Stéphane Colombi, Alexander Wiegand, Bartosz Lew, Martin Kerscher, István Szapudi, Pierre Astier, Pierre Fleury, Zachary Slepian and an anonymous referee for useful comments related to this work. Part of this work consists of research conducted within the scope of the HECOLS International Associated Laboratory, supported in part by the Polish NCN grant DEC-2013/08/M/ST9/00664. Part of this project was performed under grant 2014/13/B/ST9/00845 of the National Science Centre, Poland. BFR thanks the Centre de Recherche Astrophysique de Lyon for a warm welcome and scientifically productive hospitality. A part of this project has made use of computations made under grant 197 of the Poznań Supercomputing and Networking Center (PSNC). Some of JJO’s contributions to this work were supported by the Polish Ministry of Science and Higher Education under “Mobilność Plus II edycja”. A part of this work was conducted within the “Lyon Institute of Origins” under grant ANR-10-LABX-66. Use was made of the Centre de Données astronomiques de Strasbourg (<http://cdsads.u-strasbg.fr>), the GNU PLOTUTILS graphics package, and the GNU OCTAVE command-line, high-level numerical computation software (<http://www.gnu.org/software/octave>).

Funding for the SDSS and SDSS-II has been provided by the Alfred P. Sloan Foundation, the Participating Institutions, the National Science Foundation, the U.S. Department of Energy, the National Aeronautics and Space Administration, the Japanese Monbukagakusho, the Max Planck Society, and the Higher Education Funding Council for England. The SDSS Web Site is <http://www.sdss.org/>. The SDSS is managed by the Astrophysical Research Consortium for the Participating Institutions. The Participating Institutions are the American Museum of Natural History, Astrophysical Institute Potsdam, University of Basel, University of Cambridge, Case Western Reserve University, University of Chicago, Drexel University, Fermilab, the Institute for Advanced Study, the Japan Participation Group, Johns Hopkins University, the Joint Institute for Nuclear Astrophysics, the Kavli Institute for Particle Astrophysics and Cosmology, the Korean Scientist Group, the Chinese Academy of Sciences (LAMOST), Los Alamos National Laboratory, the Max-Planck-Institute for Astronomy (MPIA), the Max-Planck-Institute for Astrophysics (MPA), New Mexico State University, Ohio State University, University of Pittsburgh, University of Portsmouth, Princeton University, the United States Naval Observatory, and the University of Washington.

## REFERENCES

- Ade, P. A. R., Aghanim, N., Armitage-Caplan, C., et al. 2014, *A&A*, 571, A16, [arXiv:1303.5076]  
 Alexander, S., Biswas, T., Notari, A., & Vaid, D. 2009, *JCAP*, 9, 25, [arXiv:0712.0370]  
 Alnes, H., Amarzguoui, M., & Grøn, Ø. 2006, *PRD*, 73, 083519, [arXiv:astro-ph/0512006]  
 Balcerzak, A. & Dabrowski, M. P. 2013, *PRD*, 87, 063506, [arXiv:1210.6331]  
 Ballinger, W. E., Peacock, J. A., & Heavens, A. F. 1996, *MNRAS*, 282, 877, [arXiv:astro-ph/9605017]  
 Barrow, J. D., Bhavsar, S. P., & Sonoda, D. H. 1984, *MNRAS*, 210, 19P  
 Battye, R. A., Charnock, T., & Moss, A. 2014, *ArXiv e-prints*, [arXiv:1409.2769]  
 Ben-Dayan, I., Durrer, R., Marozzi, G., & Schwarz, D. J. 2014, *Physical Review Letters*, 112, 221301, [arXiv:1401.7973]  
 Biswas, T. & Notari, A. 2008, *JCAP*, 6, 21, [arXiv:astro-ph/0702555]  
 Biswas, T., Notari, A., & Valkenburg, W. 2010, *JCAP*, 11, 30, [arXiv:1007.3065]  
 Blake, C., Brough, S., Colless, M., et al. 2012, *MNRAS*, 425, 405, [arXiv:1204.3674]  
 Boehm, C. & Rasanen, S. 2013, *JCAP*, 9, 003, [arXiv:1305.7139]  
 Bolejko, K. & Célérier, M.-N. 2010, *PRD*, 82, 103510, [arXiv:1005.2584]  
 Bolejko, K., Célérier, M.-N., & Krasiński, A. 2011, *ClassQuantGra*, 28, 164002, [arXiv:1102.1449]  
 Buchert, T. 2000, in Eriguchi Y., Futamase T., Hosoya A., et al. eds, *Proceedings of the ninth workshop on general relativity and gravitation, Hiroshima November 3-6, 1999* Physics Department, Hiroshima University, Hiroshima, pp 306–321, [arXiv:gr-qc/0001056]  
 Buchert, T. 2001, *Gen. Rel. Grav.*, 33, 1381, [arXiv:gr-qc/0102049]  
 Buchert, T. 2008, *Gen. Rel. Grav.*, 40, 467, [arXiv:0707.2153]  
 Buchert, T. & Carfora, M. 2003, *Physical Review Letters*, 90, 031101, [arXiv:gr-qc/0210045]  
 Buchert, T. & Carfora, M. 2008, *ClassQuantGra*, 25, 195001, [arXiv:0803.1401]  
 Buchert, T., Kerscher, M., & Sicka, C. 2000, *PRD*, 62, 043525, [arXiv:astro-ph/9912347]  
 Buchert, T., Larena, J., & Alimi, J.-M. 2006, *ClassQuantGra*, 23, 6379, [arXiv:gr-qc/0606020]  
 Buchert, T., Nayet, C., & Wiegand, A. 2013, *PRD*, 87, 123503, [arXiv:1303.6193]  
 Buchert, T. & Ostermann, M. 2012, *PRD*, 86, 023520, [arXiv:1203.6263]  
 Célérier, M., Bolejko, K., & Krasiński, A. 2010, *A&A*, 518, A21, [arXiv:0906.0905]  
 Célérier, M.-N. 2000, *A&A*, 353, 63, [arXiv:astro-ph/9907206]  
 Chiesa, M., Maino, D., & Majerotto, E. 2014, *JCAP*, 12, 49, [arXiv:1405.7911]  
 Chuang, C.-H., Prada, F., Beutler, F., et al. 2013, *ArXiv e-prints*, [arXiv:1312.4889]  
 Clarkson, C., Clifton, T., Coley, A., & Sung, R. 2012, *PRD*, 85, 043506, [arXiv:1111.2214]  
 Cyburt, R. H., Ellis, J., Fields, B. D., et al. 2013, *JCAP*, 5, 14, [arXiv:1303.0574]  
 Cyburt, R. H., Fields, B. D., & Olive, K. A. 2008, *JCAP*, 11, 12, [arXiv:0808.2818]  
 Dabrowski, M. P. & Hendry, M. A. 1998, *ApJ*, 498, 67, [arXiv:astro-ph/9704123]  
 de Jong, R. S., Bellido-Tirado, O., Chiappini, C., et al. 2012, in McLean I. S., Ramsay S. K., Takami H., eds, *Ground-based and Airborne Instrumentation for Astronomy IV* Vol. 8446 of Society of Photo-Optical Instrumentation Engineers (SPIE) Conference Series, [arXiv:1206.6885]  
 de Lapparent, V., Geller, M. J., & Huchra, J. P. 1986, *ApJL*, 302, L1  
 Delubac, T., Bautista, J. E., Busca, N. G., et al. 2015, *A&A*, 574, A59, [arXiv:1404.1801]  
 Duley, J. A. G., Nazer, M. A., & Wiltshire, D. L. 2013, *ClassQuantGra*, 30, 175006, [arXiv:1306.3208]  
 Efron, B. 1979, *Annals of Statistics*, 7, 1, <http://projecteuclid.org/euclid.aos/1176344552>  
 Einasto, M., Lietzen, H., Tempel, E., et al. 2014, *A&A*, 562, A87, [arXiv:1401.3226]

- Eisenstein, D. J., Annis, J., Gunn, J. E., et al. 2001, *AJ*, 122, 2267, [arXiv:astro-ph/0108153]
- Eisenstein, D. J. & Hu, W. 1998, *ApJ*, 496, 605, [arXiv:astro-ph/9709112]
- Eisenstein, D. J., Zehavi, I., Hogg, D. W., et al. 2005, *ApJ*, 633, 560, [arXiv:astro-ph/0501171]
- Ellis, G. F. R. & Stoeger, W. 1987, *ClassQuantGra*, 4, 1697
- Enea Romano, A. & Chen, P. 2011, *JCAP*, 10, 16, [arXiv:1104.0730]
- Enea Romano, A., Sanes Negrete, S., Sasaki, M., & Starobinsky, A. A. 2014, *EPL (Europhysics Letters)*, 106, 69002, [arXiv:1311.1476]
- Enqvist, K. 2008, *Gen. Rel. Grav.*, 40, 451, [arXiv:0709.2044]
- Feldman, H. A., Kaiser, N., & Peacock, J. A. 1994, *ApJ*, 426, 23, [arXiv:astro-ph/9304022]
- Flender, S., Hotchkiss, S., & Nadathur, S. 2013, *JCAP*, 2, 13, [arXiv:1212.0776]
- Fleury, P., Dupuy, H., & Uzan, J.-P. 2013a, *Physical Review Letters*, 111, 091302, [arXiv:1304.7791]
- Fleury, P., Dupuy, H., & Uzan, J.-P. 2013b, *PRD*, 87, 123526, [arXiv:1302.5308]
- Futamase, T. & Sasaki, M. 1989, *PRD*, 40, 2502
- Garcia-Bellido, J. & Haugbølle, T. 2008, *JCAP*, 4, 3, [arXiv:0802.1523]
- Hampel, F. R. 1974, *Journal of the American Statistical Association*, 69, 383
- Hikage, C., Schmalzing, J., Buchert, T., et al. 2003, *PASJ*, 55, 911, [arXiv:astro-ph/0304455]
- Hosoya, A., Buchert, T., & Morita, M. 2004, *Physical Review Letters*, 92, 141302, [arXiv:gr-qc/0402076]
- Hunt, P. & Sarkar, S. 2010, *MNRAS*, 401, 547, [arXiv:0807.4508]
- Jeong, D., Dai, L., Kamionkowski, M., & Szalay, A. S. 2014, *ArXiv e-prints*, [arXiv:1408.4648]
- Kaiser, N. 1987, *MNRAS*, 227, 1
- Kasai, M. 1995, *PRD*, 52, 5605
- Kazin, E. A., Blanton, M. R., Scoccimarro, R., et al. 2010, *ApJ*, 710, 1444, [arXiv:0908.2598]
- Kerscher, M., Mecke, K., Schmalzing, J., et al. 2001, *A&A*, 373, 1, [arXiv:astro-ph/0101238]
- Kerscher, M., Szapudi, I., & Szalay, A. S. 2000, *ApJL*, 535, L13, [arXiv:astro-ph/9912088]
- Kolb, E. W. 2011, *ClassQuantGra*, 28, 164009
- Kolb, E. W. & Lamb, C. R. 2009, *ArXiv e-prints*, [arXiv:0911.3852]
- Kolb, E. W., Matarrese, S., Notari, A., & Riotto, A. 2005, *PRD*, 71, 023524, [arXiv:hep-ph/0409038]
- Kolb, E. W., Matarrese, S., & Riotto, A. 2006, *New Journal of Physics*, 8, 322, [arXiv:astro-ph/0506534]
- Landy, S. D. & Szalay, A. S. 1993, *ApJ*, 412, 64
- Larena, J., Alimi, J.-M., Buchert, T., Kunz, M., & Corasaniti, P.-S. 2009, *PRD*, 79, 083011, [arXiv:0808.1161]
- Lavinto, M., Rasanen, S., & Szybka, S. J. 2013, *ArXiv e-prints*, [arXiv:1308.6731]
- Levenberg, K. 1944, *Quarterly of Applied Mathematics*, 2, 164
- Levi, M., Bebek, C., Beers, T., et al. 2013, *ArXiv e-prints*, arXiv:1308.0847, [arXiv:1308.0847]
- Liivamägi, L. J., Tempel, E., & Saar, E. 2012, *A&A*, 539, A80, [arXiv:1012.1989]
- MacCrann, N., Zuntz, J., Bridle, S., Jain, B., & Becker, M. R. 2014, *ArXiv e-prints*, [arXiv:1408.4742]
- Marquardt, D. 1963, *J. Soc. Indust. App. Math.*, 11, 431
- Marra, V., Kolb, E. W., Matarrese, S., & Riotto, A. 2007, *PRD*, 76, 123004, [arXiv:0708.3622]
- Matsubara, T. & Suto, Y. 1996, *ApJL*, 470, L1, [arXiv:astro-ph/9604142]
- McCullagh, N., Neyrinck, M. C., Szapudi, I., & Szalay, A. S. 2013, *ApJL*, 763, L14, [arXiv:1211.3130]
- Moore, A. W., Connolly, A. J., Genovese, C., et al. 2001, in *Banday A. J., Zaroubi S., Bartelmann M., eds, Mining the Sky* p. 71, [arXiv:astro-ph/0012333]
- Moss, A., Zibin, J. P., & Scott, D. 2011, *PRD*, 83, 103515, [arXiv:1007.3725]
- Mustapha, N., Hellaby, C., & Ellis, G. F. R. 1997, *MNRAS*, 292, 817, [arXiv:gr-qc/9808079]
- Nadathur, S. & Hotchkiss, S. 2014, *MNRAS*, 440, 1248, [arXiv:1310.2791]
- Ostriker, J. P. & Steinhardt, P. J. 1995, *ArXiv Astrophysics e-prints*, [arXiv:astro-ph/9505066]
- Paraficz, D. & Hjorth, J. 2010, *ApJ*, 712, 1378, [arXiv:1002.2570]
- Räsänen, S. 2006a, *ClassQuantGra*, 23, 1823, [arXiv:astro-ph/0504005]
- Räsänen, S. 2006b, *International Journal of Modern Physics D*, 15, 2141, [arXiv:astro-ph/0605632]
- Räsänen, S. 2012, *PRD*, 85, 083528, [arXiv:1107.1176]
- Roukema, B. F. 2013, *Int. J. Mod. Phys. D*, 22, 1341018, [arXiv:1305.4415]
- Roukema, B. F., Ostrowski, J. J., & Buchert, T. 2013, *JCAP*, 10, 043, [arXiv:1303.4444]
- Roukema, B. F. & Peterson, B. A. 1994, *A&A*, 285, 361
- Saulder, C., Mieske, S., & Zeilinger, W. W. 2012, in *Dark Side of the Universe (DSU 2012)* p. 018, [arXiv:1211.1926]
- Schneider, P. 2005, in *Meylan G., Jetzer P., North P., eds, Gravitational Lensing: Strong, Weak & Micro. Lecture Notes of the 33rd Saas-Fee Advanced Course Springer-Verlag, Berlin*, p. 273, [arXiv:astro-ph/0509252]
- Sherwin, B. D. & Zaldarriaga, M. 2012, *PRD*, 85, 103523, [arXiv:1202.3998]
- Slepian, Z. & Eisenstein, D. 2015, *MNRAS*, 448, 9, [arXiv:1411.4052]
- Smale, P. R. & Wiltshire, D. L. 2011, *MNRAS*, 413, 367, [arXiv:1009.5855]
- Snethlage, M. 1999, *Metrika*, 49, 245, [arXiv:math/0002061]
- Song, Y.-S., Sabiu, C. G., Okumura, T., Oh, M., & Linder, E. V. 2014, *ArXiv e-prints*, 12, 5, [arXiv:1407.2257]
- Spergel, D. N., Verde, L., Peiris, H. V., et al. 2003, *ApJSupp*, 148, 175, [arXiv:astro-ph/0302209]
- Szybka, S. J. 2011, *PRD*, 84, 044011, [arXiv:1012.5239]
- Tomita, K. 2001, *MNRAS*, 326, 287, [arXiv:astro-ph/0011484]
- Wiegand, A., Buchert, T., & Ostermann, M. 2014, *MNRAS*, 443, 241, [arXiv:1311.3661]
- Wiltshire, D. L. 2007a, *New Journal of Physics*, 9, 377, [arXiv:gr-qc/0702082]
- Wiltshire, D. L. 2007b, *Physical Review Letters*, 99, 251101, [arXiv:0709.0732]
- Wiltshire, D. L. 2009, *PRD*, 80, 123512, [arXiv:0909.0749]
- Wiltshire, D. L., Smale, P. R., Mattsson, T., & Watkins, R. 2013, *PRD*, 88, 083529, [arXiv:1201.5371]
- Zhang, P. & Stebbins, A. 2011, *Physical Review Letters*, 107, 041301, [arXiv:1009.3967]
- Zibin, J. P. & Moss, A. 2011, *ClassQuantGra*, 28, 164005, [arXiv:1105.0909]